Journal of
Synchrotron
Radiation

ISSN 0909-0495

Received 27 January 2010
Accepted 28 May 2010

Investigation of annealing-induced oxygen vacancies in the Co-doped ZnO system by Co *K*-edge XANES spectroscopy

Shuo Zhang,[a]* Linjuan Zhang,[b] Haiming Li,[b] Jiong Li,[a,b] Zheng Jiang,[a] Wangsheng Chu,[b] Yuying Huang,[a] Jianqiang Wang[a] and Ziyu Wu[b,c]*

[a]Shanghai Synchrotron Radiation Facility, Shanghai Institute of Applied Physics, Chinese Academy of Sciences, Shanghai, People's Republic of China, [b]Beijing Synchrotron Radiation Facility, Institute of High Energy Physics, Chinese Academy of Sciences, Beijing 100049, People's Republic of China, and [c]National Synchrotron Radiation Laboratory, University of Science and Technology of China, Hefei, Anhui 230029, People's Republic of China. E-mail: zhangshuo@sinap.ac.cn, wuzy@ustc.edu.cn

To clarify the mechanism of the observed room-temperature ferromagnetism (RTF), many studies have been focused on dilute magnetic semiconductor systems. Several investigations have demonstrated that oxygen vacancies play a significant role in mediating the RTF behavior so that much effort has been devoted to confirm their presence. In this investigation, X-ray absorption spectroscopy was combined with *ab initio* calculations of the electronic structure of Co and Zn in the $Zn_{0.9}Co_{0.1}O$ system before and after annealing, which has been recognized as an effective method of originating oxygen vacancies. A feature at about 20 eV after the rising edge of the Co *K*-edge XANES that disappears after annealing has been associated with the presence of an oxygen vacancy located in the second shell surrounding the Co atom. Moreover, Zn *K*-edge XANES spectra point out that this oxygen vacancy affects the electronic structure near the Fermi level, in agreement with density functional theory calculations.

Keywords: DMS; oxygen vacancy; XANES.

1. Introduction

Since the discovery of room-temperature ferromagnetism (RTF) in dilute magnetic semiconductors (DMSs), this system has become an important research area both from the theoretical and technological points of view, because these materials are well suited for advanced spintronic devices (Wolf *et al.*, 2001; Ohno, 1998). These new magnetic semiconductors are a real challenge to understand the mechanism of RTF in condensed matter physics. In a DMS the magnetic cation's concentrations are within a few percent, a value not compatible with the existing short-range magnetic exchange interactions, such as super-exchange or double-exchange. Alternative theoretical models (Venkatesan *et al.*, 2004; Raebiger *et al.*, 2007; Kuroda *et al.*, 2007; Griffin *et al.*, 2005; Quilty *et al.*, 2006; Dietl *et al.*, 2000) have been proposed and many theoretical and experimental studies are available. However, no consensus exists on the possible mechanism at the origin of the observed RTF phenomenon.

Some contributions ascribed the origin of the RTF phase to the precipitation of magnetic clusters with the formation of a secondary magnetic phase. Others pointed out the lack of magnetic clusters or secondary phases suggesting an intrinsic origin. For instance, a carrier-mediated mechanism has been proposed to explain the RTF phenomena, although this model is not suitable for insulators which also show a RTF behavior. A bound magnetic polaron (BMP) model has also been suggested (Coey *et al.*, 2005) which foresees electrons locally trapped that occupy orbitals overlapping the *d* shells of the transition metal neighbors. In this model, oxygen vacancies play an important role in mediating the magnetic order of DMSs. Experimental investigations have been carried out to test the model while theoretical works indicate that vacancies may induce significant changes to the band structure of host oxides with a non-negligible contribution to RTF. Although it is easy to create oxygen vacancies in these systems by annealing, detection is extremely difficult because of their low amount and lack of long-range character. Conventional techniques such as X-ray diffraction are not sensitive to vacancies while X-ray absorption near-edge structure (XANES), a powerful element-selective technique, is sensitive to the three-dimensional structure around an atomic absorber, and may probe both presence and location of vacancies. Previous XANES studies investigated the atomic local struc-

ture of this system (Zhang *et al.*, 2009; Chiou *et al.*, 2006; Hsu *et al.*, 2006; Shi *et al.*, 2007; Yan *et al.*, 2007; Li *et al.*, 2006; Chang *et al.*, 2007). Hsu *et al.* (2006) showed that vacancies lead to an additional XANES feature in the pre-peak region at the Zn *K*-edge, while another investigation showed that the broadening of the white-line peak at the O *K*-edge XANES may be due to oxygen vacancies (Krishnamurthy *et al.*, 2006). However, a general consensus on these experimental results is scant because the XANES signal is due to the weighted superposition of different local and partial contributions, therefore the contribution of a few oxygen vacancies should be negligible in the *K*-edge XANES spectrum of the host element. Moreover, from previous investigations no accurate information about the locations of oxygen vacancies are available, and particularly when oxygen vacancies are localized near a magnetic ion (Weng *et al.*, 2004; Gopal & Spaldin, 2006; Patterson, 2006; Pemmaraju *et al.*, 2008). In an attempt to answer this question, we need the insight from Co *K*-edge XANES. This is a more reliable experiment because Co atoms account for a few percent in the matrix and therefore the signal induced at this edge by oxygen vacancies would be comparable.

We combined XANES experiments and multiple-scattering (MS) calculations to investigate the atomic local structure of both Co and Zn in the $Zn_{0.9}Co_{0.1}O$ system before and after annealing. The annealing treatment is recognized as an effective method of generating oxygen vacancies (Yan *et al.*, 2009; Fukuma, 2008). By the analysis of the XANES spectra of the backscattering contributions from the different coordination shells around Co atoms, we will show that the oxygen vacancy's contribution can be associated with the second shell around the magnetic atom. Additionally, we will also check results of the XANES spectra at the Zn *K*-edge.

2. Experiments and calculations

$Zn_{1-x}Co_xO$ nanocrystals were synthesized as described by Wang *et al.* (2006), by a simple solvo-thermal technique. After that, part of the samples were separated to be annealed under Ar environment at 573 K for 1 h. Co and Zn *K*-edges XANES spectra of $Zn_xCo_{1-x}O$ powders were collected at beamline 14W1 of the Shanghai Synchrotron Radiation Facility (SSRF) and at the 1W1B XAFS station of Beijing Synchrotron Radiation Facility (BSRF). For both Co and Zn *K*-edges, measurements were performed in the transmission mode. The storage ring of SSRF was working at an electron beam energy of 3.5 GeV with a maximum stored current of about 210 mA, and the storage ring of BSRF was operated at 2.5 GeV with a maximum current of about 200 mA. Data were recorded using a Si(111) double-crystal monochromator. In the energy range selected for the experiments a detuning of the silicon crystals of 30% at the Co *K*-edge and of 10% at the Zn *K*-edge was performed to suppress the high harmonics content.

XANES simulations have been performed in the framework of the MS theory (Lee & Pendry, 1975; Natoli *et al.*, 1990) using the *FEFF8.2* code (Ankudinov *et al.*, 1998). For the Co *K*-edge, calculations were performed with the structure model and the lattice parameters of the host wurtzite ZnO in which the Zn atom was replaced by a Co atom as the absorber. The *FEFF* input file was generated using the *ATOM* package for the lattice constants $a = 3.242$, $b = 3.242$ and $c = 5.206$ Å. The cluster potential was approximated by a set of spherically averaged muffin-tin (MT) potentials. For the calculations we used the Hedin–Lundqvist model (Natoli *et al.*, 1990; Tyson *et al.*, 1992). A model cluster size up to 126 atoms was used in all MS calculations to obtain an accurate self-consistent field (SCF) calculation while a larger cluster (177 atoms) was used for full multiple-scattering (FMS) calculations.

Density of states (DOS) calculations were performed using the density functional theory (DFT) as implemented in the Vienna *ab initio* simulation package (VASP) (Kresse & Hafner, 1993). The projector augmented wave was used to describe the electron–ion interaction. The local density approximation (LDA + U) has been used for the exchange-correlation function, in which U was set to 3.5 eV; a 12.5% doped ZnO has been considered to simulate the $Zn_{0.9}Co_{0.1}O$ sample. A T-centered $5 \times 5 \times 5$k mesh was used for the Brillouin zone sampling, and the electronic wavefunction was expanded using plane waves up to a cut-off energy of 500 eV.

3. Results and discussion

Fig. 1(*a*) shows experimental Co *K*-edge XANES spectra of $Zn_{0.9}Co_{0.1}O$ samples as-deposited and annealed under an Ar environment. The spectra have been normalized in the energy range 7650–7840 eV. Both spectra contain six main features labeled from *A* to *F*, similar in terms of shape and intensity, *i.e.* a weak pre-edge peak *A*, a shoulder *B* on the rising edge, a sharp white-line peak *C* followed by the weak structures *D* and *E*, and a large single scattering resonance *F*. Spectral data are affected by weak local structure effects around Co atoms induced by the annealing treatment. Indeed, a subtle but reliable difference can be detected in the region of the feature *D* before and after annealing as shown in the inset of Fig. 1(*a*). The broadening implies a local structural rearrangement around the absorber clearly associated with the annealing process. The comparison between the experimental Co *K*-edge XANES spectrum and theoretical simulations are shown in Fig. 1(*b*). Experimental data support the hypothesis that cobalt ions are homogeneously embedded in the ZnO matrix and rule out the hypothesis of the possible formation of Co clusters after annealing according to the previous investigations (Zhang *et al.*, 2009; Li *et al.*, 2006).

To recognize MS contributions originated by different shells in a XANES spectrum, we carried out calculations by using different atomic clusters around the Co absorber. Results are shown in Fig. 2(*a*). For a cluster with cobalt as the central atom, the first shell consists of four O atoms well reproducing the peak *A* and a broad peak including features *C*, *D* and *E*. Feature *A* corresponds to a dipole-allowed transition to 4*p* states hybridized with the narrow metal 3*d* band owing to the non-centrosymmetric T_d crystal field (Wu *et al.*, 2001). This feature is independent of the cluster size and reflects also its local character and the existence of a tetrahedral CoO_4 local

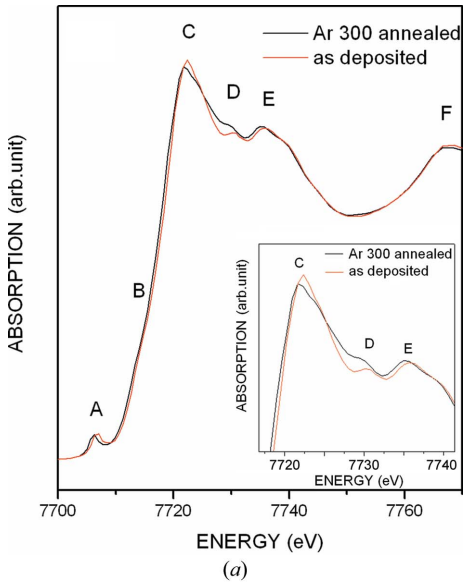

(*a*)

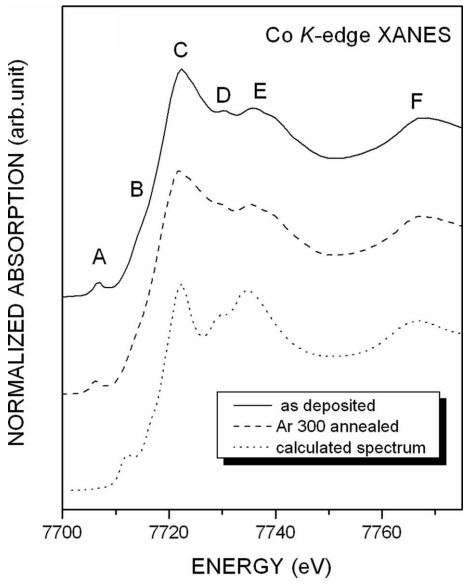

(*b*)

Figure 1
(*a*) Comparison of the Co *K*-edge XANES spectra of $Zn_{0.9}Co_{0.1}O$ before and after annealing. (*b*) Comparison of experimental and theoretical (dotted line) Co *K*-edge XANES spectra.

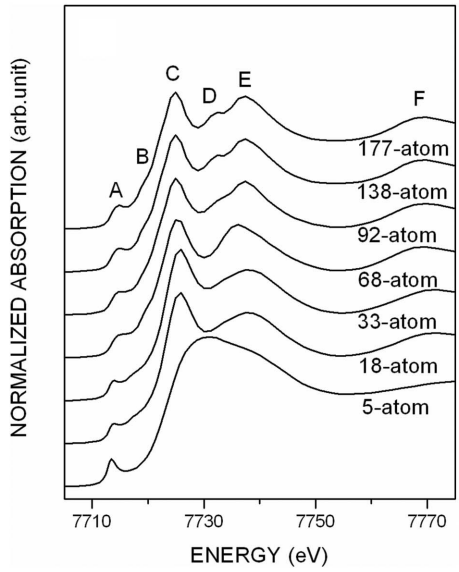

(*a*)

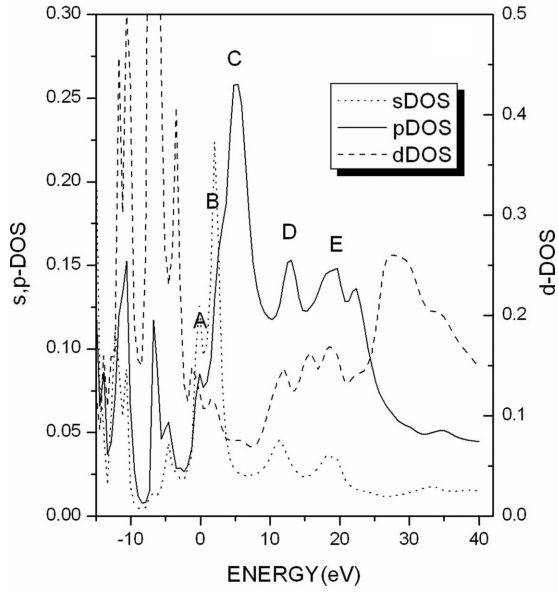

(*b*)

Figure 2
(*a*) Comparison of MS calculations for different atomic clusters of the Co *K*-edge for a Co-doped ZnO sample. (*b*) *l*-DOS for a 177-atom cluster centered at the Co site. The main spectral features, labeled *A*, *B*, *C* and *D*, are in agreement with the features in Fig. 1.

geometry. With the second shell, features *D* or *E* appear without a definite separation while the feature *B* appears only in a larger cluster with 68 atoms. Increasing the size, both feature *C* and peak *E* sharpen owing to the contribution of Co *p*-like bands. Feature *D* is separated from feature *E* only for clusters greater than 92 atoms, and becomes evident in the 133 atoms cluster, which suggests the occurrence of an effective medium-range order. Finally, a cluster of 177 atoms is sufficient to reproduce all features of the experimental spectrum. Owing to the dipole selection rules, electronic transitions appearing in the XANES spectrum at the Co *K*-edge are dominated by transitions from 1*s* to *p*-like empty states, and thus correspond quite well to the *p*-DOS shown in Fig. 2(*b*). The latter confirms quite well that the pre-edge peak is due to the contribution of Co *p* states mixed with 3*d* holes, feature *B* originates from *p*-state hybridized with *s* holes, while the white line *C* and features *D* and *E* are both dominated by empty states with a *p* character.

Based on MS calculations, we point out the important role of the second-shell atoms that contribute to the formation of both features *D* and *E*. In fact, two models can be considered to reproduce the weak local structural changes induced by the annealing treatment. The first model describing an O vacancy has an O atom missing in the second shell, while in the second model the 12 Zn atoms in the second shell are all replaced by Co. These models are shown in Figs. 3(*a*) and 3(*b*), respectively. Fig. 3(*a*) shows that the peak *D* disappears when an O atom is missing in the second shell, while the feature *E* is

independent of the O vacancy demonstrating that all (12) Zn atoms contribute to this feature. In fact, as shown in Fig. 3(*b*), the 12 cationic atoms affect the entire spectrum. In the latter we may recognize two evident changes: a widening of peak *C* and a weakening of *D* with respect to the spectrum of the ideal structure. Negligible changes are detectable for the feature *E* because both Co and Zn atoms have close atomic numbers and similar scattering amplitudes. Although we still cannot rule out contributions originating by O vacancies in other locations, these calculations illustrate that the lack of the feature *D* is compatible with an O vacancy located in the second shell around the Co ion. Therefore, we also calculated spectra with an oxygen vacancy located in different shells. Results are compared in Fig. 3(*c*) and show that only the vacancy in the second shell around Co is correlated to the feature *D*. Essentially, the feature *D* originates from MS contributions of the photoelectron by the nearest anion neighbors including four O atoms in the first coordinated shell and one O atom in the second shell. Because this peak has a relatively high frequency in *k* space, it has a long scattering path in real space. In terms of MS a missing O atom in the second shell would cancel MS contributions, leading to a strong reduction of the peak *D* in analogy with the behavior of similar post-edge peaks (Bouldin *et al.*, 1988; Tan *et al.*, 1990). In particular, Bouldin *et al.* (1988) showed that in the Ge *K*-edge spectrum of the gas-phase $GeCl_4$ a feature similar to peak *D* arises from MS contributions with the nearest chlorine neighbors. Regarding feature *E*, the discrepancy in the intensity between experimental data and theoretical calculations is an issue we extensively discussed in another manuscript. This peak originates from a MS contribution by the cationic atoms in the second coordination shell and probes the distortion of the matrix structure owing to doping.

To gain further insight into the vacancy-based model, we look at the structure around the Zn site, the other cations of the system. Zn *K*-edge XANES spectra are shown in Fig. 4(*a*). Owing to the lack of empty Zn 3*d* states, no pre-edge peak can be observed. However, attention has to be paid to the white-line feature. Indeed, looking at Fig. 4(*a*) we may see that, although with different intensities, both shape and position of the features of the two samples before and after annealing are similar. Well beyond the signal-to-noise ratio and systematic effects and in agreement with a previous investigation, the white-line amplitude decreases after annealing (Hsu *et al.*, 2006). Moreover, in a previous work it has been shown that the characteristic shape of the white line and the energy distribution of the empty *p*-like density of states are mainly determined by the number and the arrangement of the first-shell neighbors (Ławniczak-Jabłonska *et al.*, 1996). As a consequence, after annealing we have to consider the change in the amount of O vacancies around Zn atoms. Looking at the feature at the Co *K*-edge, negligible changes occur between the two samples, indicating the lack of O vacancies in the first shell surrounding the magnetic ion.

In addition, we also recognized the effect of annealing on the electronic structure near the Fermi level. By looking at the Zn *K*-edge XANES we may gain information on the bottom of the conduction band. From Fig. 4(*a*) we observe that after annealing the intensity of the white-line peak decreases dramatically. If compared with that of the as-deposited sample, there is an increase of the number of occupied Zn 4*sp* states which suggests a charge-transfer process in the annealed sample. Thus we investigated the electronic structure near the Fermi level by means of DFT calculations in which an O atom in the second shell around Co is removed. The comparison of calculations with and without O vacancies is shown in Fig. 4(*b*),

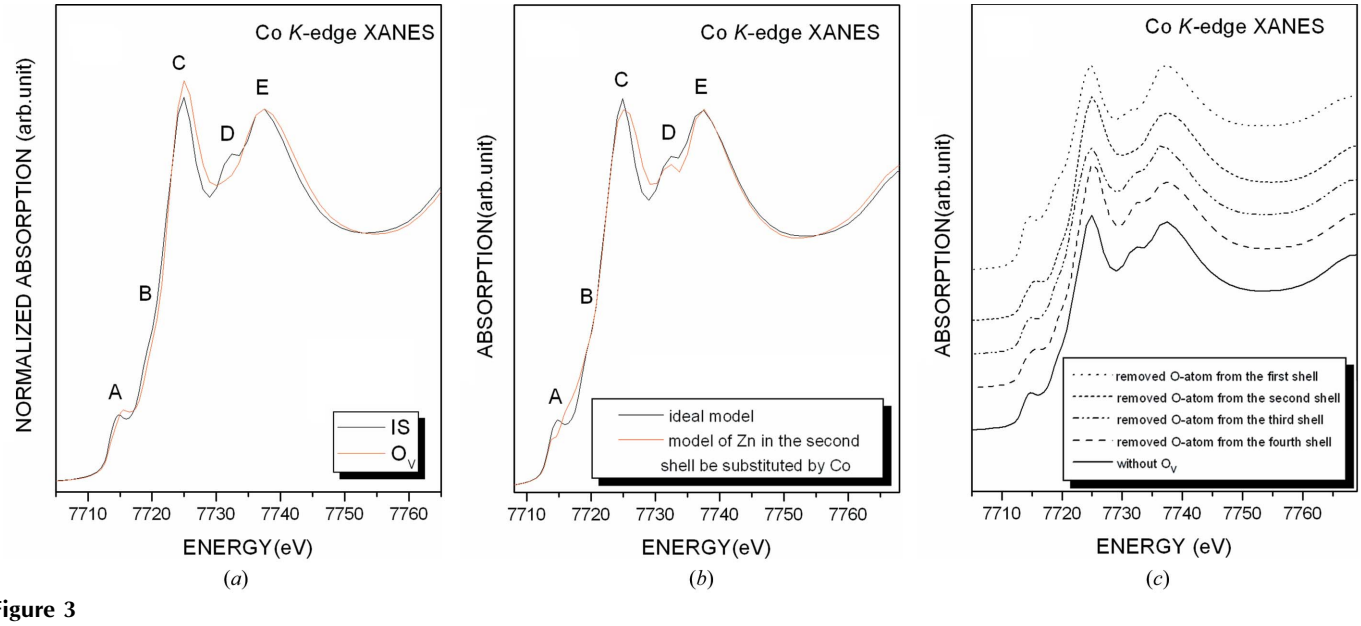

Figure 3
(*a*) Comparison of Co *K*-edge XANES spectra for different models of a Co-doped ZnO system. The ideal model (IS) consists of a Co absorber atom surrounded by the standard ZnO structure (black line), the model with an O vacancy (O_v) in which an O atom lying in the second shell is missing (red line). (*b*) Comparison of XANES spectra for the Co-doped ZnO system in the ideal model (black line) and the O-vacancy model in which 12 Zn atoms are replaced by Co atoms (red line). (*c*) Comparison of simulations with an O vacancy located in different shells around Co.

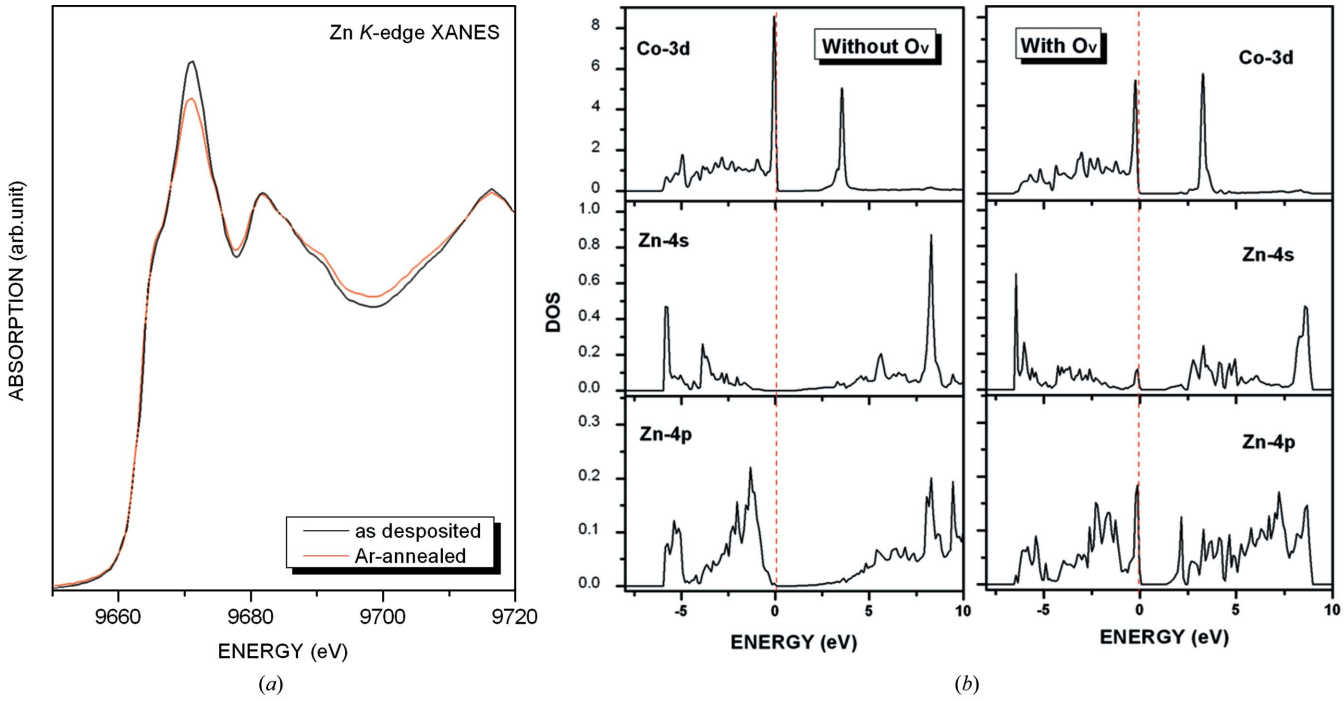

Figure 4
(*a*) Comparison of the Zn *K*-edge XANES spectra of the $Zn_{0.9}Co_{0.1}O$ sample before and after annealing. (*b*) Calculations of the partial DOS of the ZnCoO with or without O vacancies (O_v).

except for the narrower peak at 3 eV which points out minor changes occurring to the Co 3*d* partial DOS. On the contrary, several changes are evident in the Zn 4*s* and 4*p* DOS, *i.e.* relative to the DOS without vacancies:

(i) The distribution of the Zn 4*s* and 4*p* DOS with a vacancy is near to the Fermi level and supports a large overlap with Co 3*d* states. Owing to the fact that the hybridization process strongly relies on the energy difference between the two electronic states, we claim that the change induces a charge transfer process between the Co 3*d* and Zn 4*sp* states, compatible with the observed reduction of the white-line intensity at the Zn *K*-edge XANES.

(ii) An evident peak missing in the DOS without vacancies lies just at the Fermi level. The state is a possible impurity level induced by two untrapped Zn 4*s* electrons being due to an O vacancy in the second shell around Co. If we consider the BMP model, a vacancy originates two delocalized electrons (Zn 4*s* electron) that may hybridize with Co 3*d* states, forming a spin-split donor impurity band that mediates the RTF (Venkatesan *et al.*, 2004; Coey *et al.*, 2005). The analysis shows also that an O vacancy in the second shell leads to a strong hybridization between the Co 3*d* and Zn 4*sp* states. In summary, by combining data of the XANES at the Zn *K*-edge and DOS calculations, we demonstrated that also a single O vacancy may significantly affect the distribution of the Zn 4*s* states and induce a non-negligible charge transfer process.

4. Conclusions

This contribution presents an accurate XAS investigation combined with MS calculations of Co-doped ZnO samples before and after annealing. We investigated the local environment around both Co and Zn sites. The XANES analysis at the Co *K*-edge combined with calculations of different structural models shows that oxygen vacancies induced by annealing are located in the second shell around magnetic ions. The hypothesis is supported by a similar XANES analysis performed at the Zn *K*-edge. Moreover, the influence of the annealing on the electronic structure near the Fermi level is confirmed by XANES data at the Zn *K*-edge and is in agreement with DOS calculations. Results showed that an O vacancy indeed induces a strong hybridization between Co 3*d* and Zn 4*sp* states, a behavior compatible with a charge transfer process. The results are very useful for the construction of a theoretical model of the magnetic interaction in DMS materials.

This work was partly supported by the National Outstanding Youth Fund (Project No. 10125523 to ZW), by the National Natural Science Foundation of China (grant No. 10705046) and by the Knowledge Innovation Program of the Chinese Academy of Sciences (KJCX2-YW-N42). We are also grateful to A. Marcelli for many fruitful discussions.

References

Ankudinov, A. L., Ravel, B., Rehr, J. J. & Conradson, S. D. (1998). *Phys. Rev. B*, **58**, 7565–7576.
Bouldin, C. E., Bunker, G., McKeown, D. A., Forman, R. A. & Ritter, J. J. (1988). *Phys. Rev. B*, **38**, 10816–10819.
Chang, G. S., Kurmaev, E. Z., Boukhvalov, D. W., Finkelstein, L. D., Colis, S., Pedersen, T. M., Moewes, A. & Dinia, A. (2007). *Phys. Rev. B*, **75**, 195215.

Chiou, J. W., Tsai, H. M., Pao, C. W., Kumar, K. P. K., Ray, S. C., Chien, F. Z., Pong, W. F., Tsai, M. H., Chen, C. H., Lin, H. J., Wu, J. J., Yang, M. H., Liu, S. C., Chiang, H. H. & Chen, C. W. (2006). *Appl. Phys. Lett.* **89**, 043121.
Coey, J. M. D., Venkatesan, M. & Fitzgerald, C. B. (2005). *Nat. Mater.* **4**, 173–179.
Dietl, T., Ohno, H., Matsukura, F., Cibert, J. & Ferrand, D. (2000). *Science*, **287**, 1019–1022.
Fukuma, Y. (2008). *Phys. Rev. B*, **78**, 104417.
Gopal, P. & Spaldin, N. A. (2006). *Phys. Rev. B*, **74**, 094418.
Griffin, K. A., Pakhomov, A. B., Wang, C. M., Heald, S. M. & Krishnan, K. M. (2005). *Phys. Rev. Lett.* **94**, 157204.
Hsu, H. S., Huang, J. C. A., Huang, Y. H., Liao, Y. F., Lin, M. Z., Lee, C. H., Lee, J. F., Chen, S. F., Lai, L. Y. & Liu, C. P. (2006). *Appl. Phys. Lett.* **88**, 242507.
Kresse, G. & Hafner, J. (1993). *Phys. Rev. B*, **47**, 558.
Krishnamurthy, S., McGuinness, C., Dorneles, L. S., Venkatesan, M., Coey, J. M. D., Lunney, J. G., Pattersonb, C. H., Smith, K. E., Learmonth, T., Glans, P. A., Schmitt, T. & Guo, J. H. (2006). *J. Appl. Phys.* **99**, 08M111.
Kuroda, S., Nishizawa, N., Takita, K., Mitome, M., Bando, Y., Osuch, K. & Dietl, T. (2007). *Nat. Mater.* **6**, 440–446.
Ławniczak-Jabłonska, K., Iwanowski, R. J., Gołacki, Z., Traverse, A., Pizzini, S., Fontaine, A., Winter, I. & Hormes, J. (1996). *Phys. Rev. B*, **53**, 1119–1128.
Lee, P. A. & Pendry, J. B. (1975). *Phys. Rev. B*, **11**, 2795–2811.
Li, W., Kang, Q. Q., Lin, Z., Chu, W. S., Chen, D. L., Wu, Z. Y., Yan, Y., Chen, D. G. & Huang, F. (2006). *Appl. Phys. Lett.* **89**, 112507.
Natoli, C. R., Benfatto, M., Brouder, C., López, M. F. R. & Foulis, D. L. (1990). *Phys. Rev. B*, **42**, 1944–1968.
Ohno, H. (1998). *Science*, **281**, 951–956.
Patterson, C. H. (2006). *Phys. Rev. B*, **74**, 144432.
Pemmaraju, C. D., Hanafin, R., Archer, T., Braun, H. B. & Sanvito, S. (2008). *Phys. Rev. B*, **78**, 054428.
Quilty, J. W., Shibata, A., Son, J. Y., Takubo, K., Mizokawa, T., Toyosaki, H., Fukumura, T. & Kawasaki, M. (2006). *Phys. Rev. Lett.* **96**, 027202.
Raebiger, H., Lany, S. & Zunger, A. (2007). *Phys. Rev. Lett.* **99**, 167203.
Shi, T. F., Zhu, S. Y., Sun, Z. H., Wei, S. Q. & Liu, W. H. (2007). *Appl. Phys. Lett.* **90**, 102108.
Tan, Z., Filipkowski, M. E., Budnick, J. I., Heller, E. K., Brewe, D. L., Chamberland, B. L., Bouldin, C. E., Woicik, J. C. & Shi, D. (1990). *Phys. Rev. Lett.* **64**, 2715–2718.
Tyson, T. A., Hodgson, K. O., Natoli, C. R. & Benfatto, M. (1992). *Phys. Rev. B*, **46**, 5997–6019.
Venkatesan, M., Fitzgerald, C. B., Lunney, J. G. & Coey, J. M. D. (2004). *Phys. Rev. Lett.* **93**, 177206.
Wang, X. F., Xu, J. B., Zhang, B., Yu, H. G., Wang, J., Zhang, X. X., Yu, J. G. & Li, Q. (2006). *Adv. Mater.* **18**, 2476–2480.
Weng, H., Yang, X., Dong, J., Mizuseki, H., Kawasaki, M. & Kawazoe, Y. (2004). *Phys. Rev. B*, **69**, 125219.
Wolf, S. A., Awschalom, D. D., Buhrman, R. A., Daughton, J. M., von Molnar, S., Roukes, M. L., Chtchelkanova, A. Y. & Treger, D. M. (2001). *Science*, **294**, 1488–1495.
Wu, Z., Xian, D. C., Natoli, C. R., Marcelli, A., Paris, E. & Mottana, A. (2001). *Appl. Phys. Lett.* **79**, 1918–1920.
Yan, W. S., Sun, Z. H., Pan, Z. Y., Liu, Q. H., Yao, T., Wu, Z. Y., Song, C., Zeng, F., Xie, Y. N., Hu, T. D. & Wei, S. Q. (2009). *Appl. Phys. Lett.* **94**, 042508.
Yan, W., Sun, Z., Liu, Q., Li, Z., Shi, T., Wang, F., Qi, Z., Zhang, G., Wei, S., Zhang, H. & Chen, Z. (2007). *Appl. Phys. Lett.* **90**, 242509.
Zhang, S., Du, Y., Li, H., Chu, W., Li, J., Yan, W., Wei, S. & Wu, Z. (2009). *J. Phys. Chem. C*, **113**, 4263–4269.